Wave Radiation by A Submerged Ring Plate in Water of Finite Depth

Cong, Peiwen
State Key Laboratory of Coastal and Offshore Engineering, Dalian University of Technology

Liu, Yingyi
Research Institute for Applied Mechanics, Kyushu University

Gou, Ying
State Key Laboratory of Coastal and Offshore Engineering, Dalian University of Technology

Teng, Bin
State Key Laboratory of Coastal and Offshore Engineering, Dalian University of Technology

出版情報：China Ocean Engineering. 33 (6), pp.660-672, 2019-12-26. Springer Nature
バージョン：

China Ocean Eng., 2019, Vol. 33, No. 6, P. 660–672
DOI: 10.1007/s13344-019-0064-y, ISSN 0890-5487
http://www.chinaoceanengin.cn/ E-mail: coe@nhri.cn

Wave Radiation by A Submerged Ring Plate in Water of Finite Depth

CONG Pei-wen[a, b, *], LIU Ying-yi[c], GOU Ying[a], TENG Bin[a]

[a]State Key Laboratory of Coastal and Offshore Engineering, Dalian University of Technology, Dalian 116024, China

[b]Department of Civil and Environmental Engineering, National University of Singapore, 117576, Singapore

[c]Research Institute for Applied Mechanics, Kyushu University, Kasuga, Fukuoka 816-8580, Japan

Received November 14, 2018; revised May 30, 2019; accepted June 28, 2019

Abstract

A plate submerged at a certain depth underneath the sea surface has been proposed as a structure type for different purposes, including motion response reduction, wave control, and wave energy harvesting. In the present study, the three-dimensional wave radiation problem is investigated in the context of the linear potential theory for a submerged ring plate in isolation or attached to a floating column as an appendage. In the latter case, the ring plate is attached at a certain distance above the column bottom. The structure is assumed to undergo a heave motion. An analytical model is developed to solve the wave radiation problem via the eigenfunction expansion method in association with the region-matching technique. With the velocity potential being available, the hydrodynamic coefficients, such as added mass and radiation damping, are obtained through the direct pressure integration. An alternative solution of radiation damping has also been developed in this study, in which the radiation damping is related to the Kochin function in the wave radiation problem. After validating the present model, numerical analysis is performed in detail to assess the influence of various plate parameters, such as the plate size and submergence depth. It is noted that the additional added mass due to the attached ring plate is larger than that when the plate is in isolation. Meanwhile, the radiation damping of the column for the heave motion can vanish at a specific wave frequency by attaching a ring plate, corresponding to a condition that there exist no progressive waves in the exterior region.

Key words: compound structure, hydrodynamic coefficients, ring plate, zero radiation damping

Citation: Cong, P. W., Liu, Y. Y., Gou, Y., Teng, B., 2019. Wave radiation by a submerged ring plate in water of finite depth. China Ocean Eng., 33(6): 660–672, doi: 10.1007/s13344-019-0064-y

1 Introduction

A submerged plate can be frequently employed as an essential component of many offshore structures. Attaching a submerged plate to a floating system can increase the added mass and provide additional damping for the heave motion. The natural frequency of the structure can be tuned out of the dominant frequency range of incident waves, and the resonant motion response can be substantially reduced (Downie et al., 2000; Magee et al., 2000; Li et al., 2013a). Possible utilization of a submerged plate for other purposes, such as wave control and coastal morphology control, is also promising (Yip and Chwang, 1997; Yu, 2002). Besides, floating structures with attached plates have been regarded as potential wave energy harvesting devices (Orer and Ozdamar, 2007; Olaya et al., 2015; Liu et al., 2016). Therefore, the functional performance of a submerged plate is of great common interest in practical engineering.

Various studies have been performed to evaluate the hydrodynamic properties related to a submerged plate. Yu and Chwang (1993) solved the wave scattering over a submerged thin plate by means of the eigenfunction expansion matching method. Martin and Farina (1997) used the hypersingular integral equation method to examine the radiation of water waves by a heaving thin plate submerged beneath the free surface of deep water. Molin (2001) proposed a theoretical model to predict the added mass and damping of periodic arrays of plates. Tao and Thiagarajan (2003a, 2003b) studied the flow characteristics around an oscillating plate by direct numerical simulation based on the finite difference method. Farina (2010) used generalized Love's integral equation to formulate the wave radiation by a heaving horizontal plate at a shallow submergence depth. Koh and Cho (2016) provided an analytical method for simulating the wave radiation by a circular cylinder undergoing a heave motion with double thin plates. McCauley et al. (2018) applied the eigenfunction expansion method along with the transform matrix method to solve the linear diffraction and radiation problems for an arbitrary array of sub-

Foundation item: The work is financially supported by the National Natural Science Foundation of China (Grant Nos. 51809037, 51879039 and 51490672) and the Fundamental Research Funds for the Central Universities (Grant No. DUT16RC(4)048).

*Corresponding author. E-mail: pwcong@dlut.edu.cn

merged cylinders.

To maintain sustainability and stability, the motion response of a ship or an offshore structure needs to be controlled within acceptable limits. Therefore, damping elements, such as heave plates, are often used as response reduction devices in a floating system. Attaching a heave plate to the main body can increase the added mass of the structure and provide additional damping for the heave motion as well. Consequently, the hydrodynamic properties of a floating system can be changed by increasing its natural frequency in heave and introducing extra damping. Heave plates can be thin plates of circular or square shape attached at the keel of the main body or fitted beneath the main body (Downie et al., 2000; Li et al., 2013b). In the meantime, heave plates can also be ring-shaped attached at a certain distance above the keel (Koh and Cho, 2016). So far, the functional performance of submerged structures has been studied by various researchers. However, it is still necessary to understand the hydrodynamic properties of a submerged ring plate and its effects on the performance of the main structure.

The hydrodynamic analysis of an arbitrary-shaped geometry can be usually performed by a mesh-based numerical method. As to a submerged thin plate, since the vertical dimension is typically much smaller than the horizontal, a particular kind of near-singularities occur in the single- and double-layer integration kernel of $1/r$ and $1/r^2$ types (Jiang et al., 2014). To overcome this issue, a self-adaptive Gauss integral method has been developed and adopted in some studies such as Teng et al. (2010) and Ning et al. (2015). In this method, when a certain calculational element is found to be larger in size than that of the neighboring one, this element will be divided into sub-elements in a self-adaptive manner. The subdivision process does not stop until the characteristic size of the sub-element is equal to or smaller than that of the neighboring one. Then, the integral in the original element is transformed into that in the sub-elements with more Gauss points. Based on this method, high precision calculation of the nearly singular integral can be ensured.

Besides the numerical method, a substitution approach, e.g., an analytical approach, can also be effective in the hydrodynamic analysis. As the mesh generation process is not involved, the analytical approach can be free of the weakness associated with the near-singularity in the numerical method. For this reason, the analytic approach is adopted in this study to analyze the wave radiations by a submerged ring plate, within the scope of linear potential theory. In practical engineering, a submerged plate is usually used as an appendage to a floating structure. Therefore, the wave radiations by a compound structure consisting of a floating column and a ring plate attached at a certain distance above the column bottom are also concerned. The fluid domain is divided into different regions and different expansions are developed in these regions. They are matched at the conjunct bounds to determine the unknown coefficient in the expansion of the velocity potentials. Thereafter, the hydrodynamic coefficients can be obtained by integrating the fluid pressure over the body surface. Moreover, an alternative solution of radiation damping is also developed by deriving the Kochin function in the wave radiation problem. After examining the convergence and validity of the present model, detailed numerical analysis is performed, in which various plate geometric parameters are systematically adjusted to investigate their effects on the hydrodynamic coefficients.

With the introduction, the governing equation and boundary condition for the wave radiation problem is introduced. In Sections 3 and 4, hydrodynamic analysis is performed for both cases of a submerged ring plate in isolation or attached to a floating column as an appendage, respectively. In Section 5, expressions of added mass and radiation damping are given, which is followed by the convergence test and validation in Section 6. In Section 7, computed results are demonstrated and discussed. Finally, concluding remarks are given based on the previous analysis.

2 Governing equation and boundary condition

The problems of wave radiation by a submerged ring plate and a compound structure consisting of a floating column and an attached ring plate are both considered in this study. The Oxy and $Or\theta$ planes are both located on the undisturbed free surface and the z-axis points upward. The structure performs vertical oscillations of radian frequency ω and a small amplitude ξ. Then, the displacement of the motion, $\Xi(t)$, can be given as follows:

$$\Xi(t) = \mathrm{Re}\left[\xi \mathrm{e}^{-\mathrm{i}\omega t}\right], \tag{1}$$

where $\mathrm{i} = \sqrt{-1}$; Re[ ] denotes the real part of a complex expression; t is the time. It is assumed that the fluid is inviscid and incompressible, and the fluid motion is irrotational. The flow field can be described in terms of a velocity potential $\Phi(\boldsymbol{x},t)$. Based on the linear wave theory, $\Phi(\boldsymbol{x},t)$ can be reasonably expressed as:

$$\Phi(\boldsymbol{x},t) = \mathrm{Re}\left[-\mathrm{i}\omega\xi\phi(\boldsymbol{x})\mathrm{e}^{-\mathrm{i}\omega t}\right], \tag{2}$$

in which, $\phi(\boldsymbol{x})$ is the spatial part of the velocity potential and satisfies Laplace's equation,

$$\frac{\partial^2\phi(\boldsymbol{x})}{\partial r^2} + \frac{\partial\phi(\boldsymbol{x})}{r\partial r} + \frac{\partial^2\phi(\boldsymbol{x})}{r^2\partial\theta^2} + \frac{\partial^2\phi(\boldsymbol{x})}{\partial z^2} = 0, \tag{3}$$

wherever in the fluid. Besides, $\phi(\boldsymbol{x})$ is also required to satisfy appropriate boundary conditions. On the interface between air and water, the boundary condition is given as

$$\frac{\partial\phi(\boldsymbol{x})}{\partial z} = \frac{\omega^2}{g}\phi(\boldsymbol{x}) \ \text{ on } \ z=0, \tag{4}$$

in which, g is the gravity acceleration. Since no water can flow through the impermeable body surface and the sea bed, the component of the fluid velocity normal to an imper-

meable surface must be equal to the velocity of the body surface. This gives the following boundary conditions

$$\frac{\partial\phi(\boldsymbol{x})}{\partial n}=n_z \ \text{ on } \ S_\mathrm{b}, \tag{5}$$

and

$$\frac{\partial\phi(\boldsymbol{x})}{\partial z}=0 \ \text{ on } \ z=-d. \tag{6}$$

In Eq. (5), S_b represents the mean body surface; $\boldsymbol{n}=(n_x, n_y, n_z)^\mathrm{T}$ is the normal vector on S_b and is positive when pointing out of the fluid domain. In addition, $\phi(\boldsymbol{x})$ has to satisfy the Sommerfeld radiation condition at a large radial distance from the structure

$$\lim_{r\to\infty}\sqrt{\kappa_0 r}\left[\frac{\partial\phi(\boldsymbol{x})}{\partial r}-\mathrm{i}\kappa_0\phi(\boldsymbol{x})\right]=0, \tag{7}$$

in which, κ_0 is the solution of the dispersion relation $\omega^2=g\kappa_0\tanh(\kappa_0 d)$.

3 Analysis of wave radiation by a single submerged ring plate

The wave radiation by a submerged ring plate is considered firstly. The sketch of the structure is shown in Fig. 1. The submerged ring plate has an inner radius a and an outer radius R, and its axis coincides with the z-axis. The plate thickness is e. The distance between the mean free surface and the upper and bottom surfaces of the plate is denoted by d_1 and d_2, respectively. The water depth d is a constant in this study. The clearance between the plate and seabed is $S=d-d_2$.

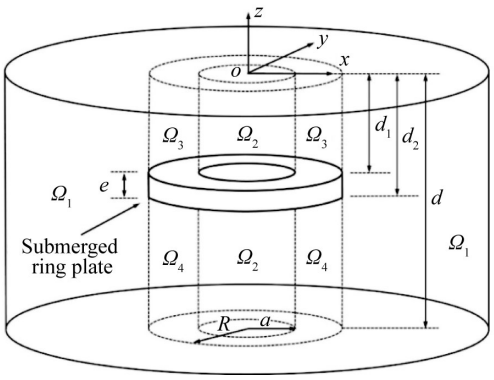

Fig. 1. Sketch of a submerged ring plate.

In the solution procedure, the whole fluid domain is divided into four subdomains denoted by Ω_1, Ω_2, Ω_3 and Ω_4 as described in Fig. 1. Ω_1 is the exterior subdomain ($r\geqslant R$, $-d\leqslant z\leqslant 0$), Ω_2 is the interior subdomain ($r\leqslant a$, $-d\leqslant z\leqslant 0$), Ω_3 is the subdomain above the plate ($a\leqslant r\leqslant R$, $-d_1\leqslant z\leqslant 0$) and Ω_4 is the subdomain below the plate ($a\leqslant r\leqslant R$, $-d\leqslant z\leqslant -d_2$). Hereinafter, $\hat{\phi}_1(\boldsymbol{x})$, $\hat{\phi}_2(\boldsymbol{x})$, $\hat{\phi}_3(\boldsymbol{x})$ and $\hat{\phi}_4(\boldsymbol{x})$ are used to denote the spatial potential in the subdomains Ω_1, Ω_2, Ω_3 and Ω_4, respectively.

The solution procedure starts from the derivation of the expressions for the velocity potential in each subdomain. Evidently, the boundary conditions on the top and bottom surfaces of the plate are inhomogeneous. Therefore, particular solutions satisfying the inhomogeneous boundary conditions are to be determined in Ω_3 and Ω_4. By using the method of separation of variables (Yeung, 1981; Mavrakos, 1985), the spatial potential can be expressed in the form of orthogonal series in each subdomain

$$\phi_1(r,z)=\sum_{j=0}^{\infty}\hat{A}_j R_j(\kappa_j r)Z_j(\kappa_j z); \tag{8a}$$

$$\hat{\phi}_2(r,z)=\sum_{j=0}^{\infty}\hat{B}_j V_j(\kappa_j r)Z_j(\kappa_j z); \tag{8b}$$

$$\hat{\phi}_3(r,z)=\sum_{j=0}^{\infty}\left[\hat{C}_j P_j(\mu_j r)+\hat{D}_j Q_j(\mu_j r)\right]U_j(\mu_j z)+\phi_{3,p}(r,z); \tag{8c}$$

$$\hat{\phi}_4(r,z)=\sum_{j=0}^{\infty}\left[\hat{E}_j S_j(\lambda_j r)+\hat{F}_j T_j(\lambda_j r)\right]Y_j(\lambda_j z)+\phi_{4,p}(r,z). \tag{8d}$$

where, $\hat{A}_j$, $\hat{B}_j$, $\hat{C}_j$, $\hat{D}_j$, $\hat{E}_j$ and $\hat{F}_j$ are unknown coefficients; $\kappa_j\,(j\geqslant 1)$ are positive real roots of $-\omega^2=g\kappa_j\tan(\kappa_j d)$; μ_0 and wave frequency ω satisfy the dispersion relation $\omega^2=g\mu_0\tanh(\mu_0 d_1)$; $\mu_j\,(j\geqslant 1)$ are positive real roots of $\omega^2=-g\mu_j\tan(\mu_j d_1)$; the eigenvalues λ_j are defined as $\lambda_0=1$ and $\lambda_j=j\pi/S$ for $j\geqslant 1$; $R_j(\kappa_j r)$, $V_j(\kappa_j r)$, $S_j(\lambda_j r)$ and $T_j(\lambda_j r)$ are radial functions, and defined by the following equations

$$R_j(\kappa_j r)=\begin{cases}\mathrm{H}_0(\kappa_0 r), & j=0\\ \mathrm{K}_0(\kappa_j r), & j\geqslant 1\end{cases} \tag{9a}$$

$$V_j(\lambda_l r)=\begin{cases}\mathrm{J}_0(\kappa_0 r), & j=0\\ \mathrm{I}_0(\kappa_j r), & j\geqslant 1\end{cases} \tag{9b}$$

$$S_j(\lambda_j r)=\begin{cases}\dfrac{\ln(R/r)}{\ln(R/a)}, & j=0\\ \dfrac{\mathrm{K}_0(\lambda_j r)\mathrm{I}_0(\lambda_j R)-\mathrm{K}_0(\lambda_j R)\mathrm{I}_0(\lambda_j r)}{\mathrm{K}_0(\lambda_j a)\mathrm{I}_0(\lambda_j R)-\mathrm{K}_0(\lambda_j R)\mathrm{I}_0(\lambda_j a)}, & j\geqslant 1\end{cases} \tag{9c}$$

$$T_j(\lambda_j r)=\begin{cases}\dfrac{\ln(r/a)}{\ln(R/a)}, & j=0\\ \dfrac{\mathrm{K}_0(\lambda_j a)\mathrm{I}_0(\lambda_j r)-\mathrm{K}_0(\lambda_j r)\mathrm{I}_0(\lambda_j a)}{\mathrm{K}_0(\lambda_j a)\mathrm{I}_0(\lambda_j R)-\mathrm{K}_0(\lambda_j R)\mathrm{I}_0(\lambda_j a)}, & j\geqslant 1\end{cases} \tag{9d}$$

In Eq. (9), $\mathrm{H}_0(x)$ is the Hankel function of the first kind of zeroth order; $\mathrm{I}_0(x)$ and $\mathrm{K}_0(x)$ are the modified Hankel functions of the first and second kinds of zeroth order, respectively. The expression of $P_j(\mu_j r)$ and $Q_j(\mu_j r)$ can be determined according to Eqs. (9a) and (9b), respectively,

with κ_j replaced by μ_j. $Z_j(\kappa_j z)$, $U_j(\mu_j z)$ and $Y_j(\lambda_j z)$ are orthonormal functions given at the intervals $[-d, 0]$, $[-d_1, 0]$ and $[-d, -d_2]$, respectively, and defined as:

$$Z_j(\kappa_j z)=\begin{cases}\dfrac{\cosh[\kappa_0(z+d)]}{\cosh(\kappa_0 d)}, & j=0\\ \dfrac{\cos[\kappa_j(z+d)]}{\cos(\kappa_j d)}, & j\geqslant 1\end{cases} \tag{10a}$$

$$U_j(\mu_j z)=\begin{cases}\dfrac{\cosh[\mu_0(z+d_1)]}{\cosh(\mu_0 d_1)}, & j=0\\ \dfrac{\cos[\mu_j(z+d_1)]}{\cos(\mu_j d_1)}, & j\geqslant 1\end{cases} \tag{10b}$$

$$Y_j(\lambda_j z)=\begin{cases}\dfrac{\sqrt{2}}{2}, & j=0\\ \cos[\lambda_j(z+d)], & j\geqslant 1\end{cases} \tag{10c}$$

The particular solutions in Eqs. (8c) and (8d), $\phi_{3,p}(r,z)$ and $\phi_{4,p}(r,z)$, are derived as:

$$\phi_{3,p}(r,z)=z+\frac{1}{v_0}; \tag{11a}$$

$$\phi_{4,p}(r,z)=\frac{1}{2S}\left[(z+d)^2-\frac{r^2}{2}\right], \tag{11b}$$

in which, v_0 is the deep-water wave number and defined as ω^2/g.

These expressions are developed to satisfy Laplace's equation and all boundary conditions. In addition, these expressions have to satisfy the condition of the continuity of pressure and normal velocity at the borders between two neighboring subdomains, i.e., $r = R$ and $r = a$. To find a solution to these coefficients, the infinite series of orthogonal functions has to be truncated and in Eq. (8) only the first N terms are taken.

The continuity of the normal velocity between different subdomains at $r = R$ and $r = a$ can be satisfied over the z interval in the least-square manner by making use of the orthogonal properties of the vertical eigenfunctions. The procedure can give the following two sets of linear equations with $0 \leqslant j, l \leqslant N$–1

$$\sum_{l=0}^{N-1}\left(G_{j,l}\hat{A}_l+G_{j,2N+l}\hat{C}_l+G_{j,3N+l}\hat{D}_l+G_{j,4N+l}\hat{E}_l+G_{j,5N+l}\hat{F}_l\right)=Y_j; \tag{12a}$$

$$\sum_{l=0}^{N-1}\left(G_{N+j,N+l}\hat{B}_l+G_{N+j,2N+l}\hat{C}_l+G_{N+j,3N+l}\hat{D}_l+G_{N+j,4N+l}\hat{E}_l+G_{N+j,5N+l}\hat{F}_l\right)=Y_{N+j}, \tag{12b}$$

in which,

$$G_{j,l}=\begin{cases}\kappa_j R'_j(\kappa_j R)N_j(\kappa_j d), & j=l\\ 0, & j\neq l\end{cases} \tag{13a}$$

$$G_{j,2N+l}=-\alpha_{j,l}\mu_l P'_l(\mu_l r)\big|_{r=R}; \tag{13b}$$

$$G_{j,3N+l}=-\alpha_{j,l}\mu_l Q'_l(\mu_l r)\big|_{r=R}; \tag{13c}$$

$$G_{j,4N+l}=-\beta_{j,l}\lambda_l S'_l(\lambda_l r)\big|_{r=R}; \tag{13d}$$

$$G_{j,5N+l}=-\beta_{j,l}\lambda_l T'_l(\lambda_l r)\big|_{r=R}; \tag{13e}$$

$$Y_j=\int_{-d}^{-d_2}Z_j(\kappa_j z)\phi'_{4,p}(r,z)\big|_{r=R}\mathrm{d}z; \tag{13f}$$

$$G_{N+j,N+l}=\begin{cases}\kappa_j V'_j(\kappa_j a)N_j(\kappa_j d), & j=l\\ 0, & j\neq l\end{cases} \tag{13g}$$

The definition of $G_{N+j,2N+l}$, $G_{N+j,3N+l}$, $G_{N+j,4N+l}$, $G_{N+j,5N+l}$ and Y_{N+j} can be obtained according to Eqs. (13b), (13c), (13d), (13e) and (13f), respectively, with $r = a$. In Eq. (13), the prime denotes the derivative with respect to the argument; $N_j(\kappa_j d)$ represents the inner products of the eigenfunction $Z_j(\kappa_j z)$, and is defined as:

$$N_j(\kappa_j d)=\int_{-d}^{0}Z_j^2(\kappa_j z)\mathrm{d}z=\begin{cases}\dfrac{1}{\cosh^2(\kappa_0 d)}\dfrac{d}{2}\left[1+\dfrac{\sinh(2\kappa_0 d)}{2\kappa_0 d}\right], & j=0\\ \dfrac{1}{\cos^2(\kappa_j d)}\dfrac{d}{2}\left[1+\dfrac{\sin(2\kappa_j d)}{2\kappa_j d}\right], & j\geqslant 1\end{cases} \tag{14}$$

The coefficients $\alpha_{j,l}$ and $\beta_{j,l}$ are defined as:

$$\alpha_{j,l}=\int_{-d_1}^{0}Z_j(\kappa_j z)U_l(\mu_l z)\mathrm{d}z; \tag{15a}$$

$$\beta_{j,l}=\int_{-d}^{-d_2}Z_j(\kappa_j z)Y_l(\lambda_l z)\mathrm{d}z. \tag{15b}$$

By matching the potential between different subdomains at $r = R$ and $r = a$ and using the orthogonal properties of the vertical eigenfunctions $U_j(\mu_j z)$ and $Y_j(\lambda_j z)$, the following four sets of linear equations with $0 \leqslant j, l \leqslant N$–1 can be obtained

$$\sum_{l=0}^{N-1}\left(G_{2N+j,N+l}\hat{B}_l+G_{2N+j,2N+l}\hat{C}_l+G_{2N+j,3N+l}\hat{D}_l\right)=Y_{2N+j}; \tag{16a}$$

$$\sum_{l=0}^{N-1}\left(G_{3N+j,l}\hat{A}_l+G_{3N+j,2N+l}\hat{C}_l+G_{3N+j,3N+l}\hat{D}_l\right)=Y_{3N+j}; \tag{16b}$$

$$\sum_{l=0}^{N-1}\left(G_{4N+j,N+l}\hat{B}_l+G_{4N+j,4N+l}\hat{E}_l\right)=Y_{4N+j}; \tag{16c}$$

$$\sum_{l=0}^{N-1}\left(G_{5N+j,l}\hat{A}_l+G_{5N+j,5N+l}\hat{F}_l\right)=Y_{5N+j}, \tag{16d}$$

in which,

$$G_{2N+j,N+l} = \alpha_{l,j} V_l(\kappa_l r)|_{r=a}; \tag{17a}$$

$$G_{2N+j,2N+l} = -\begin{cases} N_j(\mu_j d_1)\, P_j(\mu_j r)\big|_{r=a}, & j = l \\ 0, & j \neq l \end{cases} \tag{17b}$$

$$G_{2N+j,3N+l} = -\begin{cases} N_j(\mu_j d_1)\, Q_j(\mu_j r)\big|_{r=a}, & j = l \\ 0, & j \neq l \end{cases} \tag{17c}$$

$$Y_{2N+j} = \int_{-d_1}^{0} U_j(\mu_j z)\, \phi_{3,p}(r,z)\big|_{r=a} \mathrm{d}z; \tag{17d}$$

$$G_{3N+j,l} = \alpha_{l,j} R_l(\kappa_l r)|_{r=R}, \tag{17e}$$

and

$$G_{4N+j,N+l} = \beta_{l,j} V_l(\kappa_l r)|_{r=a}; \tag{18a}$$

$$G_{4N+j,4N+l} = G_{5N+j,5N+l} = -\begin{cases} \dfrac{S}{2}, & j = l \\ 0, & j \neq l \end{cases} \tag{18b}$$

$$Y_{4N+j} = \int_{-d}^{-d_2} Y_j(\lambda_j z)\, \phi_{4,p}(r,z)\big|_{r=a} \mathrm{d}z; \tag{18c}$$

$$G_{5N+j,l} = \beta_{l,j} R_l(\kappa_l r)|_{r=R}. \tag{18d}$$

The definition of $G_{3N+j,2N+l}$, $G_{3N+j,3N+l}$, Y_{3N+j} and Y_{5N+j} can be obtained according to Eqs. (17b), (17c), (17d) and (18c), respectively, with $r = R$. In Eq. (17), $N_j(\mu_j d_1)$ represents the inner products of the eigenfunction $U_j(\mu_j z)$ and is defined as:

$$N_j(\mu_j d_1) = \int_{-d_1}^{0} U_j^2(\mu_j z)\mathrm{d}z = \begin{cases} \dfrac{1}{\cosh^2(\mu_0 d_1)} \dfrac{d_1}{2}\left[1 + \dfrac{\sinh(2\mu_0 d_1)}{2\mu_0 d_1}\right], & j = 0 \\ \dfrac{1}{\cos^2(\mu_j d_1)} \dfrac{d_1}{2}\left[1 + \dfrac{\sin(2\mu_j d_1)}{2\mu_j d_1}\right], & j \geqslant 1 \end{cases} \tag{19}$$

We now obtain six sets of the linear system of $6N$ complex equations and an equal number of unknown coefficients. The linear equations in Eqs. (12) and (17) can be resembled as:

$$\boldsymbol{G}_{6N\times 6N}\boldsymbol{X}_{6N} = \boldsymbol{Y}_{6N}, \tag{20}$$

in which, $\boldsymbol{X}$ consists of the unknown coefficients $\hat{A}_j$, $\hat{B}_j$, $\hat{C}_j$, $\hat{D}_j$, $\hat{E}_j$ and $\hat{F}_j$. For the definition of $\boldsymbol{G}$ and $\boldsymbol{Y}$, please refer to Eqs. (13), (16) and (17). Solving the linear algebraic systems gives the unknown coefficients in the orthogonal series. Then, the velocity potential at any position in the fluid domain can be obtained.

4 Analysis of wave radiation by a compound structure consisting of a submerged ring plate and a floating column

The wave radiation by a compound structure consisting of a circular column and an attached ring plate is then considered. The sketch of the compound structure is shown in Fig. 2. A circular column with radius a and draft T is floating in the fluid and its axis coincides with the z-axis. The ring plate is coaxial with the column. The clearance between the column and seabed is $S_1 = d - T$.

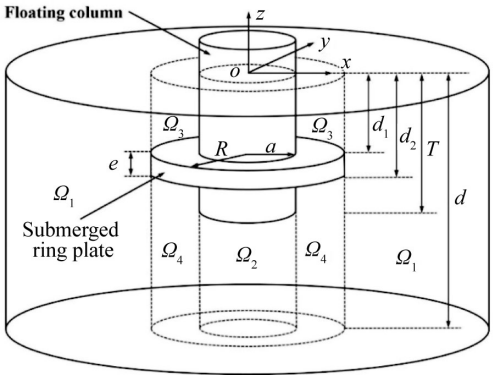

Fig. 2. Sketch of a compound structure.

The whole fluid domain is divided into four subdomains, i.e., Ω_1, Ω_2, Ω_3 and Ω_4, as shown in Fig. 2. Ω_1 is the exterior subdomain ($r \geqslant R$, $-d \leqslant z \leqslant 0$), Ω_2 is the interior subdomain ($r \leqslant a$, $-d \leqslant z \leqslant -T$), Ω_3 is the subdomain above the plate ($a \leqslant r \leqslant R$, $-d_1 \leqslant z \leqslant 0$) and Ω_4 is the subdomain below the plate ($0 \leqslant r \leqslant R$, $-d \leqslant z \leqslant -d_2$). Hereinafter, ϕ_n (n = 1, 2, 3, 4) is used to denote the spatial potential in these subdomains.

We proceed to obtain the expressions of the spatial potential. By using the method of separation of variables, the velocity potential valid in each subdomain can be expressed as follows:

$$\phi_1(r,z) = \sum_{j=0}^{\infty} \widehat{A}_j R_j(\kappa_j r) Z_j(\kappa_j z); \tag{21a}$$

$$\phi_2(r,z) = \sum_{j=0}^{\infty} \widehat{B}_j O_j(\gamma_j r) W_j(\gamma_j z) + \phi_{2,p}(r,z); \tag{21b}$$

$$\phi_3(r,z) = \sum_{j=0}^{\infty} \left[\widehat{C}_j P_j(\mu_j r) + \widehat{D}_j Q_j(\mu_j r)\right] U_j(\mu_j z) + \phi_{3,p}(r,z); \tag{21c}$$

$$\phi_4(r,z) = \sum_{j=0}^{\infty} \left[E_j S_j(\lambda_j r) + F_j T_j(\lambda_j r)\right] Y_j(\lambda_j z) + \phi_{4,p}(r,z). \tag{21d}$$

In Eq. (21), $\widehat{A}_j$, $\widehat{B}_j$, $\widehat{C}_j$ and $\widehat{D}_j$ are unknown coefficients; the eigenvalues γ_j are defined as $\gamma_0 = 1$ and $\gamma_j = j\pi/S_1$ for $j \geqslant 1$; the radial function $O_j(\gamma_j r)$ and vertical function $W_j(\gamma_j z)$ are defined by

$$O_j(\gamma_j r) = \begin{cases} 1, & j = 0 \\ \dfrac{\mathrm{I}_0(\gamma_j r)}{\mathrm{I}_0(\gamma_j a)}, & j \geqslant 1 \end{cases} \tag{22}$$

and

$$W_j\left(\gamma_j z\right)=\begin{cases}\dfrac{\sqrt{2}}{2}, & j=0\\ \cos\left[\gamma_j(z+d)\right], & j\geqslant 1\end{cases} \tag{23}$$

Other radial and vertical functions, such as $R_j\left(\kappa_j r\right)$, $P_j\left(\mu_j r\right)$, $Q_j\left(\mu_j r\right)$, $S_j\left(\lambda_j r\right)$, $T_j\left(\lambda_j r\right)$, $Z_j\left(\kappa_j z\right)$ and $Y_j\left(\lambda_j z\right)$, have been defined in Eqs. (9) and (10), respectively. Owing to the inhomogeneous body-surface conditions, particular solutions, $\phi_{2,p}(r,z)$, $\phi_{3,p}(r,z)$ and $\phi_{4,p}(r,z)$, are expected in subdomains Ω_2, Ω_3 and Ω_4. $\phi_{3,p}(r,z)$ and $\phi_{4,p}(r,z)$ have been defined in Eq. (11). $\phi_{2,p}(r,z)$ is then given by

$$\phi_{2,p}(r,z)=\frac{1}{2S_1}\left[(z+d)^2-\frac{r^2}{2}\right]. \tag{24}$$

The velocity potential given in Eq. (21) describes the flow in the respective region. The unknown coefficients in these expressions can be determined by imposing the matching condition at $r=R$ and $r=a$, based on the assumption that the fluid pressure and the normal velocity are continuous across the border of neighboring subdomains. After truncating the infinite series of the orthogonal functions in Eq. (21) to finite terms, i.e. N terms, six sets of linear equations can be established containing an equivalent number of unknown coefficients. After solving the linear algebraic system, the unknown coefficients are found and the velocity potential in each subdomain is obtained.

5 Calculation of the hydrodynamic coefficients

Once the solution has been obtained for the velocity potential, the pressure distribution can be determined immediately according to the Bernoulli equation. The hydrodynamic force caused by the motion of the structure can be achieved by integrating the fluid pressure over the body surface. The added mass is defined as a quantity giving the part of the hydrodynamic force on the body which is in phase with the acceleration of the moving body. Similarly, the radiation damping is defined as a quantity giving the part of the hydrodynamic force in phase with the velocity of the moving body. For the case of a submerged ring plate in isolation, the added mass and radiation damping due to the heave motion, a_{33} and b_{33}, can be determined according to

$$a_{33}+\frac{\mathrm{i}b_{33}}{\omega}=\hat{f}_3+\hat{f}_4, \tag{25}$$

in which

$$\hat{f}_3=2\pi\rho\left[\sum_{j=0}^{N-1}\left(\hat{\Pi}_{1,j}+\hat{\Pi}_{2,j}\right)-\frac{1}{2}\left(-d_1+\frac{1}{v_0}\right)\left(R^2-a^2\right)\right]; \tag{26a}$$

$$\hat{f}_4=2\pi\rho\left[\sum_{j=0}^{N-1}\left(\hat{\Pi}_{3,j}+\hat{\Pi}_{4,j}\right)+\frac{S}{4}\left(R^2-a^2\right)-\frac{1}{16S}\left(R^4-a^4\right)\right]. \tag{26b}$$

In Eq. (26),

$$\hat{\Pi}_{1,j}=\begin{cases}-\dfrac{\hat{C}_0}{\mu_0}\dfrac{\Lambda_{1,0}}{\cosh(\mu_0 d_1)}, & j=0\\ -\dfrac{\hat{C}_j}{\mu_j}\dfrac{\Lambda_{1,j}}{\cos(\mu_0 d_1)}, & j\geqslant 1\end{cases} \tag{27a}$$

$$\hat{\Pi}_{2,j}=\begin{cases}-\dfrac{\hat{D}_0}{\mu_0}\dfrac{\Lambda_{2,0}}{\cosh(\mu_0 d_1)}, & j=0\\ -\dfrac{\hat{D}_j}{\mu_j}\dfrac{\Lambda_{2,j}}{\cos(\mu_0 d_1)}, & j\geqslant 1\end{cases} \tag{27b}$$

$$\hat{\Pi}_{3,j}=\begin{cases}-\dfrac{\sqrt{2}}{2}\dfrac{\hat{E}_0}{\ln(R/a)}\left[\dfrac{1}{2}a^2\ln(R/a)-\dfrac{1}{4}R^2+\dfrac{1}{4}a^2\right], & j=0\\ -\dfrac{\hat{E}_j}{\lambda_j}\dfrac{\mathrm{K}_0\left(\lambda_j R\right)\Lambda_{4,j}-\Lambda_{3,j}\mathrm{I}_0\left(\lambda_j R\right)}{\mathrm{K}_0\left(\lambda_j a\right)\mathrm{I}_0\left(\lambda_j R\right)-\mathrm{K}_0\left(\lambda_j R\right)\mathrm{I}_0\left(\lambda_j a\right)}(-1)^j, & j\geqslant 1\end{cases} \tag{27c}$$

$$\hat{\Pi}_{4,j}=\begin{cases}\dfrac{\sqrt{2}}{2}\dfrac{\hat{F}_0}{\ln(R/a)}\left[\dfrac{1}{2}R^2\ln(R/a)-\dfrac{1}{4}R^2+\dfrac{1}{4}a^2\right], & j=0\\ \dfrac{\hat{F}_j}{\lambda_j}\dfrac{\mathrm{K}_0\left(\lambda_j a\right)\Lambda_{4,j}-\Lambda_{3,j}\mathrm{I}_0\left(\lambda_j a\right)}{\mathrm{K}_0\left(\lambda_j a\right)\mathrm{I}_0\left(\lambda_j R\right)-\mathrm{K}_0\left(\lambda_j R\right)\mathrm{I}_0\left(\lambda_j a\right)}(-1)^j, & j\geqslant 1\end{cases} \tag{27d}$$

and

$$\Lambda_{1,j}=\begin{cases}\mathrm{H}_1(\mu_0 R)R-\mathrm{H}_1(\mu_0 a)a, & j=0\\ -\mathrm{K}_1\left(\mu_j R\right)R+\mathrm{K}_1\left(\mu_j a\right)a, & j\geqslant 1\end{cases} \tag{28a}$$

$$\Lambda_{2,j}=\begin{cases}\mathrm{J}_1(\mu_0 R)R-\mathrm{J}_1(\mu_0 a)a, & j=0\\ \mathrm{I}_1\left(\mu_j R\right)R-\mathrm{I}_1\left(\mu_j a\right)a, & j\geqslant 1\end{cases} \tag{28b}$$

$$\Lambda_{3,j}=-\mathrm{K}_1\left(\lambda_j R\right)R+\mathrm{K}_1\left(\lambda_j a\right)a, \quad j\geqslant 1; \tag{28c}$$

$$\Lambda_{4,j}=\mathrm{I}_1\left(\lambda_j R\right)R-\mathrm{I}_1\left(\lambda_j a\right)a, \quad j\geqslant 1. \tag{28d}$$

Similarly, for the case of a submerged ring plate attached to a floating column as an appendage, the hydrodynamic coefficients due to the heave motion can be determined according to

$$a_{33}+\frac{\mathrm{i}b_{33}}{\omega}=\widehat{f}_2+\widehat{f}_3+\widehat{f}_4, \tag{29}$$

in which,

$$\widehat{f}_2=2\pi\rho\left[\widehat{B}_0\frac{\sqrt{2}}{4}a^2+\sum_{j=1}^{N-1}\widehat{B}_j\frac{\mathrm{I}_1\left(\mu_j a\right)a}{\mathrm{I}_0\left(\mu_j a\right)\mu_j}(-1)^j+\frac{1}{2S_1}\left(\frac{1}{2}a^2S_1^2-\frac{1}{8}a^4\right)\right]; \tag{30a}$$

$$\widehat{f}_3=2\pi\rho\left[\sum_{j=0}^{N-1}\left(\widehat{\Pi}_{1,j}+\widehat{\Pi}_{2,j}\right)-\frac{1}{2}\left(-d_1+\frac{1}{v_0}\right)\left(R^2-a^2\right)\right]; \tag{30b}$$

$$\widehat{f}_4=2\pi\rho\left[\sum_{j=1}^{N-1}\left(\widehat{\Pi}_{3,j}+\widehat{\Pi}_{4,j}\right)+\frac{S}{4}\left(R^2-a^2\right)-\frac{1}{16S}\left(R^4-a^4\right)\right]. \tag{30c}$$

In Eq. (30), $\widehat{\Pi}_{1,j}$, $\widehat{\Pi}_{2,j}$, $\widehat{\Pi}_{3,j}$ and $\widehat{\Pi}_{4,j}$ can be determined

according to Eq. (27) with $\hat{C}_j$ and $\hat{D}_j$ replaced by $\widehat{C}_j$ and $\widehat{D}_j$, respectively.

6 Convergence test and validation

Convergence test on the added mass and radiation damping concerning the truncation number of eigenmodes N is performed. In Figs. 3 and 4, the added mass and radiation damping are depicted as a function of N at $\kappa_0 a = 1$ and 2 for both cases of a ring plate in isolation (see Fig. 3) or attached to a floating column as an appendage (see Fig. 4). The value presented in Figs. 3 and 4 is the ratio of $a_{33}(N)/a_{33}^*$ or $b_{33}(N)/b_{33}^*$, in which a_{33}^* and b_{33}^* are the added mass and radiation damping with $N = 200$, respectively. It can be found that $N = 100$ can guarantee the convergence of the results for the test case. In the meantime, for most cases we tested, $N = 100$ is an appropriate value to truncate the series taking into account both the convergence and computational cost. Thus, $N = 100$ is adopted in the subsequent parametric study.

Besides the direct pressure integration, it is also possible to derive an alternative solution of radiation damping in the following manner. The case of a submerged ring plate as shown in Fig. 1 is concerned first. A finite fluid volume Ω_c comprising S_b, S_c, S_f' and S_d' is considered, in which S_c is the control surface surrounding the body and defined by $r = R_c$ and $-d \leqslant z \leqslant 0$; S_f' and S_d' are the limited mean free surface and seabed inside Ω_c. According to Mei et al. (2005), the application of Green's second identity in Ω_c and the use of the boundary conditions of Eqs. (4), (5) and (6) give

$$\iint_{S_b} (\phi - \phi^*) n_z \mathrm{d}s = -\iint_{S_c} \left(\phi \frac{\partial \phi^*}{\partial r} - \phi^* \frac{\partial \phi}{\partial r} \right) \mathrm{d}s, \tag{31}$$

in which, * denotes the complex conjugate. Eq. (31) suggests that

$$b_{33} = \frac{1}{2} \mathrm{i}\omega\rho \iint_{S_c} \left(\phi \frac{\partial \phi^*}{\partial r} - \phi^* \frac{\partial \phi}{\partial r} \right) \mathrm{d}s. \tag{32}$$

The velocity potential in the exterior region is given by Eq. (8a). By inserting Eq. (8a) into the right-hand side of Eq. (32) and applying the orthogonal relationship, Eq. (32) can be rewritten as:

$$b_{33} = -2\omega\rho\pi \mathrm{Im}\left[\hat{A}_0 \hat{A}_0^* \kappa_0 R_c \mathrm{H}_0(\kappa_0 R_c) \frac{\partial \mathrm{H}_0^*(\kappa_0 R_c)}{\partial(\kappa_0 R_c)} N_0(\kappa_0 d) + \sum_{j=1}^{\infty} \hat{A}_j \hat{A}_j^* \kappa_j R_c \mathrm{K}_j(\kappa_j R_c) \frac{\partial \mathrm{K}_j(\kappa_j R_c)}{\partial(\kappa_j R_c)} N_j(\kappa_j d) \right], \tag{33}$$

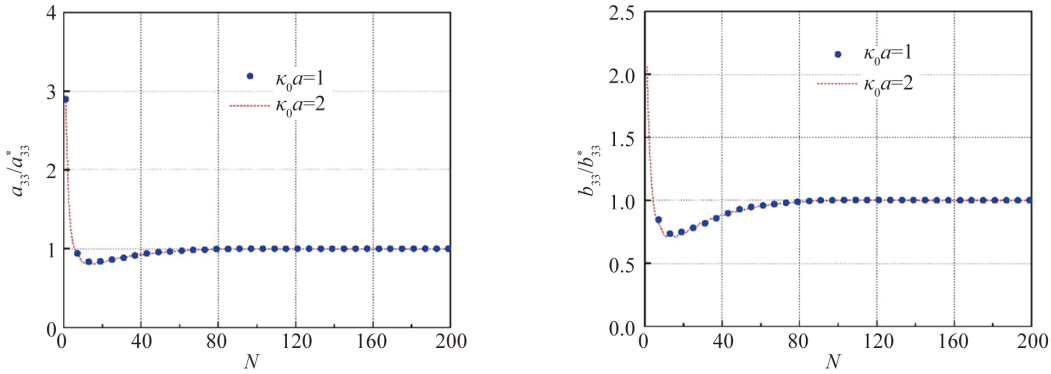

Fig. 3. Convergence test on the added mass and radiation damping for the case of a submerged ring plate ($R = 1.5a$, $e = 0.1a$, $d_2 = 2a$ and $d = 10a$) at $\kappa_0 a = 1.0$.

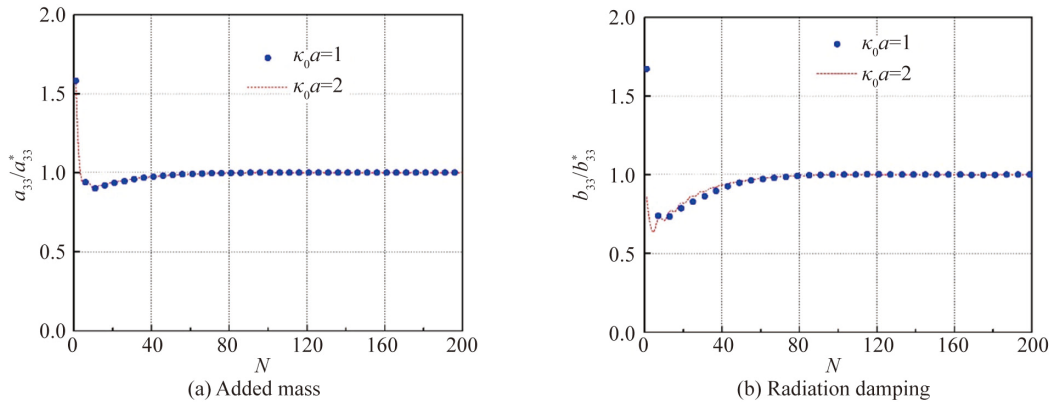

Fig. 4. Convergence test on the added mass and radiation damping for the case of a compound structure ($R = 1.5a$, $e = 0.1a$, $d_2 = 2a$, $T = 3a$ and $d = 10a$).

in which, 'Im' indicates that the imagery part is taken. If the control surface S_c is moved to infinity, the contribution from the evanescent modes to the velocity potential can be neglected. By using the asymptotic expressions for Bessel functions, the velocity potential for large $\kappa_0 r$ can be expressed in an asymptotic form. That is

$$\phi_1(r,z)=\hat{A}_0\sqrt{\frac{2}{\pi\kappa_0 r}}e^{i(\kappa_0 r-\pi/4)}Z_0(\kappa_0 d)+O\left[(\kappa_0 r)^{-3/2}\right], \quad (34)$$

as $\kappa_0 r$ tends to infinity. In Eq. (34), $\hat{A}_0$ has been defined as the radiation Kochin function in some previous studies, such as Zhao et al. (2011), that is, the angular variation of the radially spreading waves at far field. In this study, $\hat{A}_0$ is independent of θ, due to the axisymmetric mode of motion and the axisymmetry of the structure. Then, after inserting Eq. (34) into Eq. (32), it can be obtained that

$$b_{33}=4\omega\rho\hat{A}_0\hat{A}_0^* N_0(\kappa_0 d). \quad (35)$$

Eq. (35) gives the relationship between the Kochin function and the heave radiation damping. In addition, it provides an alternative solution of radiation damping. Eq. (35) is also applicable for the case of a compound structure as shown in Fig. 2 after replacing $\hat{A}_0$ by A_0.

In order to make sure that the developed analytical model is valid and reliable to a convinced degree, a comparison between the radiation damping based on the pressure integration (see Eqs. (25) and (29)) and that based on the alternative solution (see Eq. (35)) is made. From the comparison in Figs. 5 and 6, it is evident that the results achieved by different methods are in good agreement.

7 Numerical results and discussion

To understand the effects of the plate geometric parameters on the hydrodynamic coefficients, numerical studies are carried out in detail for both the cases of a ring plate in isolation or attached to a floating column as an appendage. In all calculations, the draft of the column T and the wave depth d are fixed at $3a$ and $10a$, respectively.

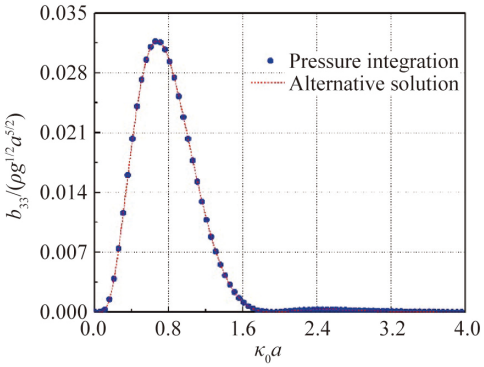

Fig. 5. Comparative results of radiation damping for the case of a submerged ring plate in isolation ($R=1.5a$, $e=0.1a$, $d_2=2a$ and $d=10a$).

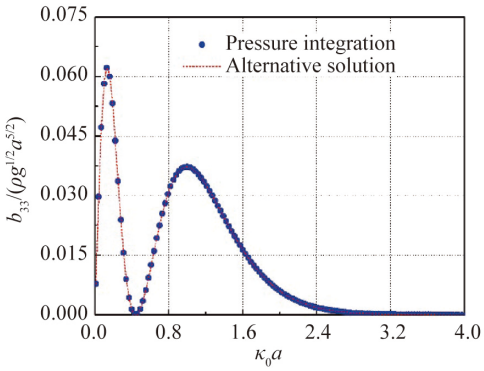

Fig. 6. Comparative results of radiation damping for the case of a compound structure ($R=1.5a$, $e=0.1a$, $d_2=2a$, $T=3a$ and $d=10a$).

7.1 Effects of the plate draft

The effects of the plate draft on the hydrodynamic coefficients are shown in Fig. 7 for the case of a submerged ring plate with $e=0.2a$ and $R=1.5a$. Meanwhile, the plate draft is varied as $d_2=1.5a$, $1.75a$, $2a$, $2.25a$ and $2.5a$. It is noted that the added mass is hardly affected by the plate draft (see Fig. 7a). If the plate is moved closer to the free surface, the motion of the plate can generate more outgoing waves. As a

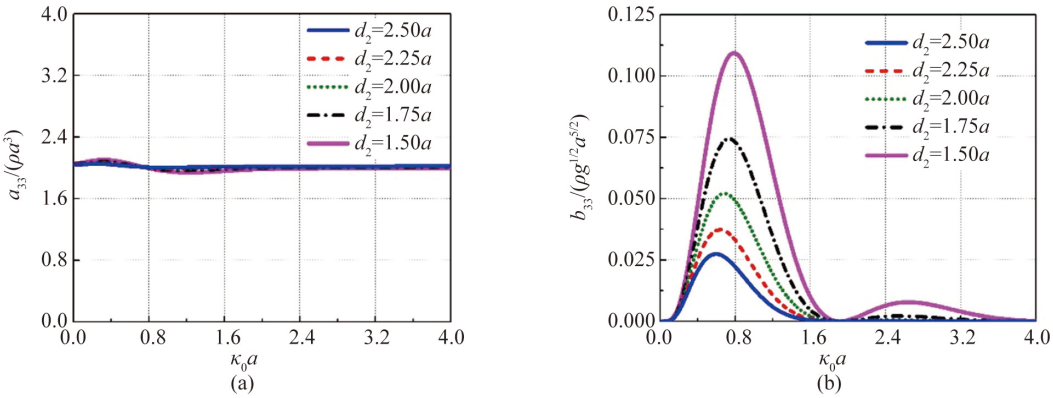

Fig. 7. Dimensionless added mass and radiation damping of a submerged ring plate in correspondence to various plate drafts ($R=1.5a$, $e=0.2a$ and $d=10a$).

result, a decrease of the plate draft can give rise to a substantial enhancement of the radiation damping (see Fig. 7b). In Fig. 7b, an obvious zero-damping frequency can be observed around $\kappa_0 a = 1.912$ when $d_2 = 1.5a$. As the radiation damping is closely related to the progressive waves in the exterior region, the variation of outgoing waves along the radial direction is examined for this specific wave frequency. After obtaining the velocity potential, the linear radiation waves, ζ_0, can be immediately determined according to

$$\zeta_0(t) = -\frac{1}{\mathrm{i}\omega}\frac{\partial \Phi(t)}{\partial z} = \mathrm{Re}\left[\eta_0 \mathrm{e}^{-\mathrm{i}\omega t}\right]. \tag{36}$$

When the wave radiation by a submerged ring plate is considered, the outgoing waves are driven by the fluxes emitted from the regions above and under the plate. As a result, the overall wave elevation can be further expressed as:

$$\zeta_0(t) = \zeta_1(t) + \zeta_2(t) = \mathrm{Re}\left[(\eta_1 + \eta_2)\mathrm{e}^{-\mathrm{i}\omega t}\right]. \tag{37}$$

in which, ζ_1. and ζ_2 represent the wave elevation due to the vertical movement of the upper and bottom surfaces of the plate, respectively. In Eqs. (36) and (37), η_i (i = 0, 1, 2) is the complex amplitude of the wave elevation ζ_i. For the case of a submerged ring plate, the variation of η_0, η_1 and η_2 along the radial direction is given in Fig. 8 with $\kappa_0 a = 1.912$ and $d_2 = 1.5a$. In the meantime, the time history of the wave elevation at $r = 15L$ with $\kappa_0 a = 1.912$ and $d_2 = 1.5a$ is given in Fig. 9, in which L is the wave length and equal to $2\pi/\kappa_0$. In Figs. 8 and 9, the values are all nondimensionalized by $\xi\sqrt{a/r}$. The progressive waves decay at a rate of $1/\sqrt{r}$ (see Eq. (34)) at far field. Therefore, in Fig. 8, the dimensionless value with i = 1 or 2 tends to a constant as r tends to infinity. In the meantime, the overall wave elevation decays quickly as r increases until it vanishes. Fig. 9 reveals that even though ζ_1. and ζ_2 are with the same magnitude at far field, they are out-of-phase. As a result, there exist no progressive waves in the exterior region at this specific wave frequency, leading to no radiation damping.

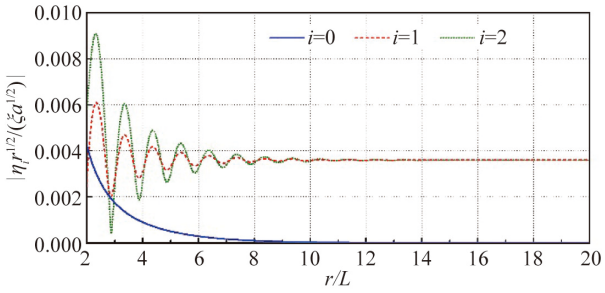

Fig. 8. Dimensionless wave elevation amplitude along the radial direction at $\kappa_0 a = 1.912$ for the case of a submerged ring plate ($R = 1.5a$, $e = 0.2a$, $d_2 = 1.5a$ and $d = 10a$).

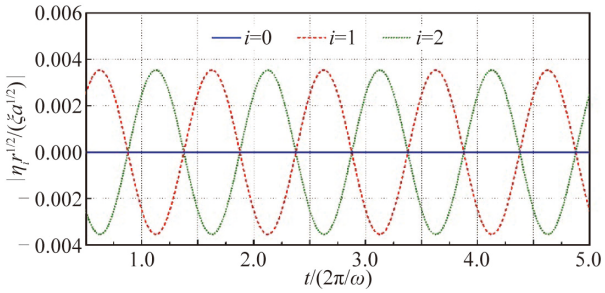

Fig. 9. Time history of the dimensionless wave elevation at $r = 15L$ with $\kappa_0 a = 1.912$ for the case of a submerged ring plate ($R = 1.5a$, $e = 0.2a$, $d_2 = 1.5a$ and $d = 10a$).

The effects of the plate draft on the hydrodynamic coefficients are shown in Fig. 10 for the case of a compound structure with $e = 0.2a$ and $R = 1.5a$. In Fig. 10a, the added mass in general increases as the plate draft increases at a fixed wave frequency. This is because more fluid can be entrapped in the region above the plate as the plate draft increases. In Fig. 10b, obvious zero-damping frequencies, at which the structure radiates no energy outward in the heave motion, can be observed. Before the zero-damping frequency, the plate draft has negligible effects on the radiation damping. When beyond that, attaching a plate at relatively shallower submergence can produce a larger amount

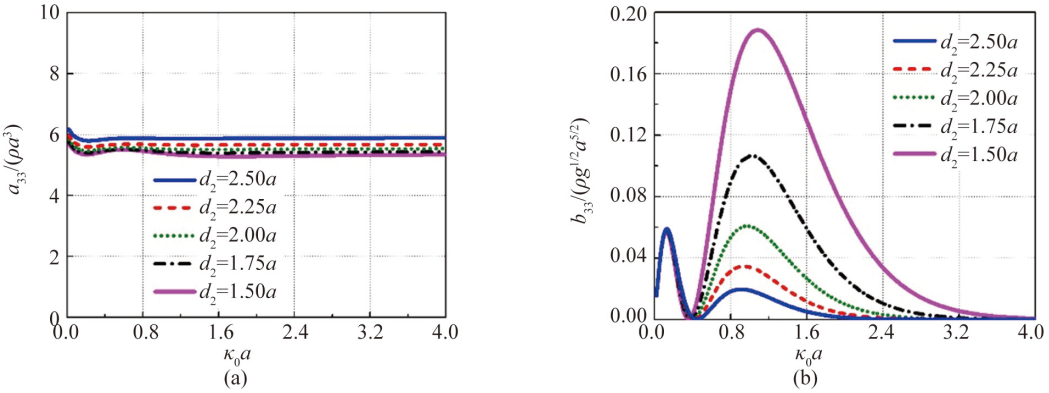

Fig. 10. Dimensionless added mass and radiation damping of a compound structure in correspondence to various plate drafts ($R = 1.5a$, $e = 0.2a$, $T = 3a$ and $d = 10a$).

of radiation damping. When the wave radiation by a compound structure is considered, the overall wave elevation contains the contribution due to the motion of the plate, ζ_1. and ζ_2, as well as that due to the motion of the column, ζ_3. Then, we can obtain

$$\zeta_0(t)=\zeta_1(t)+\zeta_2(t)+\zeta_3(t)=\mathrm{Re}\left[(\eta_1+\eta_2+\eta_3)\mathrm{e}^{-\mathrm{i}\omega t}\right]. \quad (38)$$

The variation of the wave elevation amplitude η_0, η_1, η_2 and η_3 along the radial direction is given in Fig. 11 for the case of a compound structure with $\kappa_0 a = 0.358$ and $d_2 = 1.5a$. In the meantime, the time history of the wave elevation at $r = 15L$ with $\kappa_0 a = 0.358$ and $d_2 = 1.5a$ is given in Fig. 12. In Fig. 11, the dimensionless value with $i = 1$, 2 or 3 tends to a constant as r tends to infinity. From Fig. 12, it is noted that at far field, the wave elevation driven by the vertical movement of the upper surface of the plate, i.e., ζ_1, is always out-of-phase with those due to the vertical movements of the bottom surface of the plate and column, ζ_2 and ζ_3. Owing to the phase cancellation between ζ_1, ζ_2 and ζ_3, the overall wave elevation vanishes at far field at this specific wave frequency. As a result, there exist no progressive waves in the exterior region, leading to no radiation damping. The above explanation is also applicable to the occurrence of other zero radiation damping for the case of a compound structure. We also note that a decrease of the plate draft can lead to a small shift of the zero-damping frequency to the low-frequency region. This is because moving the plate closer to free surface can enhance the wave elevation ζ_1. Then, at the far-field region, ζ_1 can balance ζ_2 and ζ_3 at an earlier wave frequency.

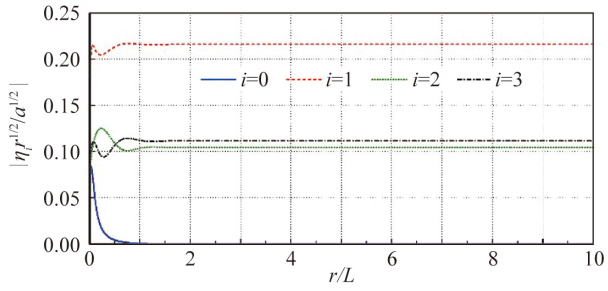

Fig. 11. Dimensionless wave elevation amplitude along the radial direction at $\kappa_0 a = 0.358$ for the case of a compound structure ($R = 1.5a$, $e = 0.2a$, $d_2 = 1.5a$, $T = 3a$ and $d = 10a$).

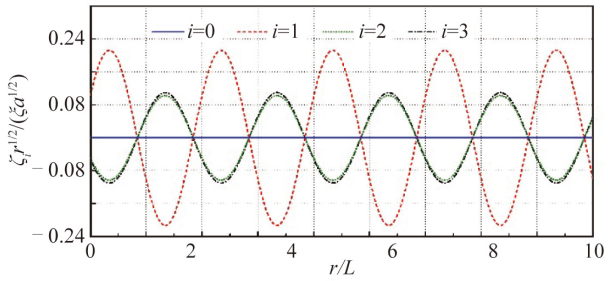

Fig. 12. Time history of the dimensionless wave elevation at $r = 15L$ with $\kappa_0 a = 0.358$ for the case of a compound structure ($R = 1.5a$, $e = 0.2a$, $d_2 = 1.5a$, $T = 3a$ and $d = 10a$).

7.2 Effects of the plate radius

The effects of the plate radius on the hydrodynamic coefficients are then investigated and the numerical results are presented in Figs. 13 and 14. In these calculations, the plate thickness and plate draft are fixed at $e = 0.2a$ and $d_2 = 2a$, respectively. Meanwhile, the outer radius of the ring plate is varied as $R = a$, $1.2a$, $1.4a$, $1.5a$ and $1.6a$.

Fig. 13 presents the variation of the added mass and radiation damping with respect to various outer radii of the plate for the case of a submerged ring plate. In Fig. 13a, regardless of the value of R, the added mass a_{33} behaves stable in the whole frequency range. An increase of R can lead to an obvious increase of a_{33}. This is because the plate can be surrounded by more fluid as its outer radius increases. In Fig. 13b, each curve is characterized by an obvious peak around $\kappa_0 a = 0.68$. As the outer radius of the plate increases, more free-surface kinetic energy transformation can be caused, leading to more progressive waves in the exterior region. Therefore, the radiation damping increases as R increases at a certain wave frequency.

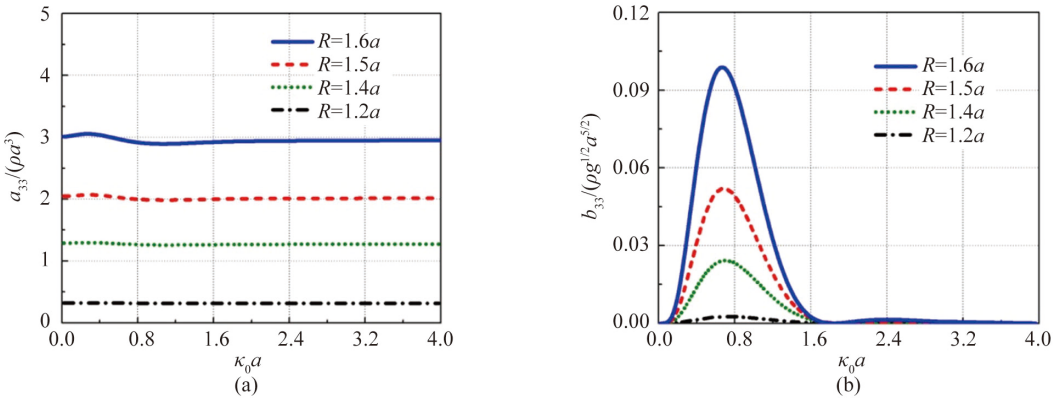

Fig. 13. Dimensionless added mass and radiation damping of a submerged ring plate in correspondence to various outer radii of the plate ($d_2 = 2a$, $e = 0.2a$ and $d = 10a$).

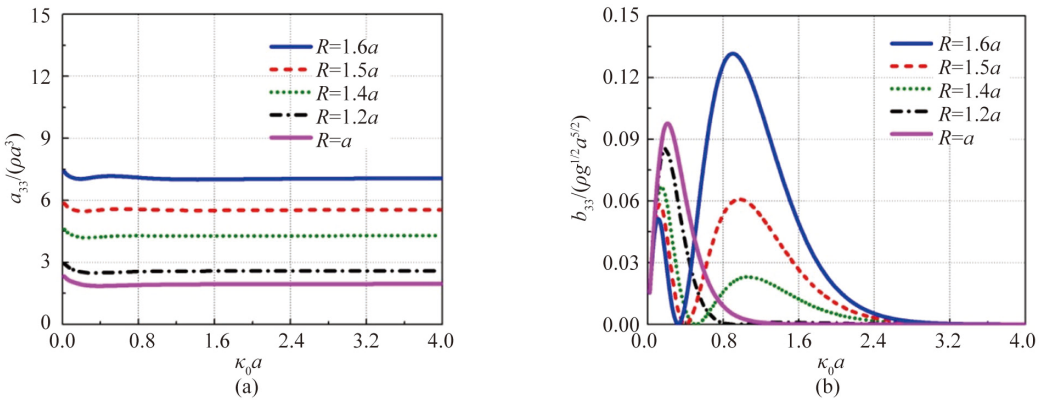

Fig. 14. Dimensionless added mass and radiation damping of a compound structure in correspondence to various outer radii of the plate ($d_2 = 2a$, $e = 0.2a$, $T = 3a$ and $d = 10a$).

Fig. 14 presents the variation of the hydrodynamic coefficients with respect to various outer radii of the attached plate for the case of a compound structure. In Fig. 14, $R = a$ corresponds to the case without an attached plate, i.e., a single column. In Fig. 14a, a remarkable increase of the added mass, which is almost constant and independent of $\kappa_0 a$, can be induced by an increase of R. The added mass with $r > a$ is obviously larger than that with $r = a$. It suggests that attaching a ring plate to a floating system can increase the added mass for the heave motion, thereby shifting the natural frequency out of the wave energy regime. It is also noted that the additional added mass due to the attached plate is substantially larger than that when the plate is in isolation. For example, at $\kappa_0 a = 1$, the dimensionless added mass of a floating column increases from 1.920 to 5.532 after attaching a ring plate of $R = 1.5a$ to it. Meanwhile, when the plate is in isolation, the dimensionless added mass at $\kappa_0 a = 1$ is only 1.986 (see Fig. 13a). This is because waves can be entrapped in the regions above and below the plate after attaching a plate to the column. In Fig. 14b, the curves corresponding to $R > a$ show a more complex tendency than that of $R = a$, as there exists an obvious zero-damping frequency. In the high-frequency region, a floating column with an attached plate ($R > a$) can generate significantly more radiation damping for the heave motion than that without an attached plate ($R = a$) and is therefore more effective in suppressing the motion. However, around the zero-damping frequency, a floating column with an attached plate ($R > a$) can generate obviously less radiation damping than that without an attached plate ($R = a$). It illustrates that attaching a ring plate to a floating column does not always enhance the radiation damping. When a floating column experiences excessive heave motion around the zero-damping frequency, attaching a ring plate to the column can cause a lack of radiation damping. From the aspect of radiation damping, the ring plate should be carefully used around the zero-damping frequency. As the outer radius of the plate increases, the wave elevation due to the vertical movement of the upper surface of the plate, ζ_1, can be obviously enhanced. Then, at the far-field region, ζ_1 can balance the opposite contribution to the wave elevation, ζ_2 and ζ_3, at an earlier wave frequency. Therefore, the zero-damping frequency moves gradually to the low-frequency region as the outer radius of the plate increases.

7.3 Effects of the plate thickness

The effects of the plate thickness on the hydrodynamic coefficients are presented in Figs. 15 and 16. In the following calculations, the outer radius and draft of the plate are fixed at $R = 1.5a$ and $d_2 = 2a$, respectively. Meanwhile, the plate thickness is varied as $e = 0$, $0.1a$, $0.2a$, $0.3a$ and $0.4a$.

Fig. 15 presents the variation of the added mass and radiation damping for different plate thicknesses for the case of a submerged ring plate. The added mass and radiation damping both increase as e increases at a certain wave frequency. As the plate height increases, the plate can more effectively interact with surface waves. Therefore, the effects of the plate thickness get more pronounced as its upper surface gets closer to the free surface (e increases).

Fig. 16 presents the variation of the hydrodynamic coefficients with respect to the change of the plate thickness for the case of a compound structure. In Fig. 16a, an increase of the plate thickness can give rise to an almost constant increase of the added mass. In Fig. 16b, again the radiation damping vanishes at a specific frequency. Before the zero-damping frequency, the influence of the plate thickness on b_{33} is trivial. While beyond that, b_{33} becomes quite sensitive to the plate thickness and a small increase of e can lead to a pronounced increase of b_{33}. As the upper surface of the plate gets closer to the free surface (e increases), the wave elevation due to the vertical movement of the upper surface of the plate, ζ_1, can be enhanced. Then, at the far-field region, ζ_1 can balance the other contribution to the wave elevation, ζ_2 and ζ_3, at an earlier wave frequency. Therefore, the zero-damping frequency moves gradually to the low-frequency region as e increases.

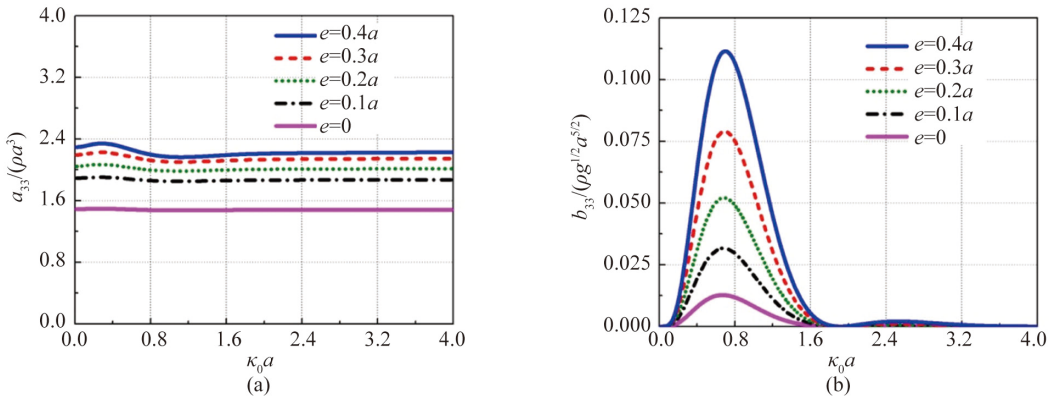

Fig. 15. Dimensionless added mass and radiation damping of a submerged ring plate in correspondence to different plate thicknesses ($d_2 = 2a$, $R = 1.5a$, $d = 10a$).

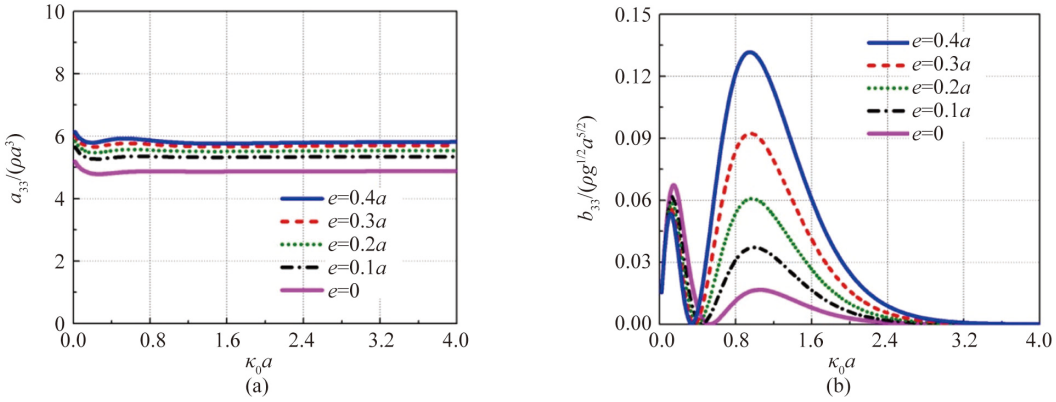

Fig. 16. Dimensionless added mass and radiation damping of a compound structure in correspondence to different plate thicknesses ($d_2 = 2a$, $R = 1.5a$, $d = 10a$).

8 Conclusions

The wave radiation problems have been investigated in the context of the linear potential theory for both cases of a ring plate in isolation or attached to a floating column as an appendage. The structure is assumed to undergo a heave motion and an analytical model is developed to solve the wave radiation problem based on the eigenfunction expansion matching method. Detailed numerical studies are performed to understand the effects of the plate geometric parameters. The main conclusions of this study can be summarized as follows.

(1) The present analytical model is validated by comparing the radiation damping based on different methods, and good agreement has been found.

(2) The change of the plate size can result in a noticeable impact on the added mass and radiation damping. Whether a ring plate is in isolation or attached to a floating column, an increase of the outer radius or thickness of the plate can lead to the rise of the added mass and the radiation damping. For a submerged ring plate, the plate submergence has little effect on the added mass which remains almost the same as the plate gets closer to the free surface. However, moving the ring plate closer to the free surface can produce more damping effects for the heave motion. When a ring plate is attached to a floating column, the added mass gradually decreases as the submergence depth decreases. Also, beyond the zero-damping frequency, attaching the plate at shallower submergence can generate a more considerable amount of radiation damping for the heave motion.

(3) Attaching a ring plate to a floating column can increase the added mass. However, it does not always increase the radiation damping. The additional added mass due to the attached ring plate is significantly larger than that when the plate is in isolation. The radiation damping for the heave motion can vanish at a specific wave frequency after attaching a ring plate to the column. This is resulted from the possible phase cancellation between the outgoing waves due to the motions of the column and the plate. The progressive waves in the exterior region can vanish at a specific wave frequency, leading to zero radiation damping. The zero damping can also be found for a submerged ring plate. This is because the vertical movements of the upper and bottom surfaces of the plate can generate progressive waves of the same magnitude but out-of-phase in the exterior region at a specific wave frequency.

References

Downie, M.J., Graham, J.M.R., Hall, C., Incecik, A. and Nygaard, I., 2000. An experimental investigation of motion control devices for truss spars, *Marine Structures*, 13(2), 75–90.

Farina, L., 2010. Water wave radiation by a heaving submerged horizontal disk very near the free surface, *Physics of Fluids*, 22(5), 057102.

Jiang, S.C., Gou, Y. and Teng, B., 2014. Water wave radiation problem by a submerged cylinder, *Journal of Engineering Mechanics*, 140(5), 06014003.

Koh, H.J. and Cho, I.H., 2016. Heave motion response of a circular cylinder with the dual damping plates, *Ocean Engineering*, 125, 95–102.

Li, B.B., Huang, Z.H., Low, Y.M. and Ou, J.P., 2013a. Experimental and numerical study of the effects of heave plate on the motion of a new deep draft multi-spar platform, *Journal of Marine Science and Technology*, 18(2), 229–246.

Li, J.X., Liu, S.X., Zhao, M. and Teng, B., 2013b. Experimental investigation of the hydrodynamic characteristics of heave plates using forced oscillation, *Ocean Engineering*, 66, 82–91.

Liu, K., Liang, H.Z. and Ou, J.P., 2016. Numerical investigation of a tuned heave plate energy-harvesting system of a semi-submersible platform, *Energies*, 9(2), 82.

Magee, A., Sablok, A., Maher, J., Halkyard, J., Finn, L. and Datta, I., 2000. Heave plate effectiveness in the performance of truss spars, *Proceedings of ETCE/OMAE 2000 Joint Conference*, ASME, New Orleans, USA.

Martin, P.A. and Farina, L., 1997. Radiation of water waves by a heaving submerged horizontal disc, *Journal of Fluid Mechanics*, 337, 365–379.

Mavrakos, S.A., 1985. Wave loads on a stationary floating bottomless cylindrical body with finite wall thickness, *Applied Ocean Research*, 7(4), 213–224.

McCauley, G., Wolgamot, H., Orszaghova, J. and Draper, S., 2018. Linear hydrodynamic modelling of arrays of submerged oscillating cylinders, *Applied Ocean Research*, 81, 1–14.

Mei, C.C., Stiassnie, M. and Yue, D.K.P., 2005. *Theory and Applications of Ocean Surface Waves*, World Scientific, Singapore.

Molin, B., 2001. On the added mass and damping of periodic arrays of fully or partially porous disks, *Journal of Fluids and Structures*, 15(2), 275–290.

Ning, D.Z., Shi, J., Zou, Q.P. and Teng, B., 2015. Investigation of hydrodynamic performance of an OWC (oscillating water column) wave energy device using a fully nonlinear HOBEM (higher-order boundary element method), *Energy*, 83, 177–188.

Olaya, S., Bourgeot, J.M. and Benbouzid, M.E.H., 2015. Hydrodynamic coefficient computation for a partially submerged wave energy converter, *IEEE Journal of Oceanic Engineering*, 40(3), 522–535.

Orer, G. and Ozdamar, A., 2007. An experimental study on the efficiency of the submerged plate wave energy converter, *Renewable Energy*, 32(8), 1317–1327.

Tao, L.B. and Thiagarajan, K., 2003a. Low KC flow regimes of oscillating sharp edges I. Vortex shedding observation, *Applied Ocean Research*, 25(1), 21–35.

Tao, L.B. and Thiagarajan, K., 2003b. Low KC flow regimes of oscillating sharp edges. II. Hydrodynamic forces, *Applied Ocean Research*, 25(2), 53–62.

Teng, B., Zheng, M.Z., Jiang, S.C., Gou, Y. and Lu, L., 2010. Calculation and analysis of the hydrodynamic coefficients of heave-plates of Spar platform, *The Ocean Engineering*, 28(3), 1–8. (in Chinese)

Yeung, R.W., 1981. Added mass and damping of a vertical cylinder in finite-depth waters, *Applied Ocean Research*, 3(3), 119–133.

Yip, T.L. and Chwang, A.T., 1997. Water wave control by a pitching plate, *Journal of Engineering Mechanics*, 123(8), 800–807.

Yu, X.P., 2002. Functional performance of a submerged and essentially horizontal plate for offshore wave control: A review, *Coastal Engineering Journal*, 44(2), 127–147.

Yu, X.P. and Chwang, A.T., 1993. Analysis of wave scattering by submerged circular disk, *Journal of Engineering Mechanics*, 119(9), 1804–1817.

Zhao, F.F., Kinoshita, T., Bao, W.G., Wan, R., Liang, Z.L. and Huang, L.Y., 2011. Hydrodynamics identities and wave-drift force of a porous body, *Applied Ocean Research*, 33(3), 169–177.